

## Article

# A Statistical Risk Assessment Model of the Hazard Chain Induced by Landslides and Its Application to the Baige Landslide

Feng-Yuan Yang , Li Zhuo \*, Ming-Li Xiao, Hong-Qiang Xie, Huai-Zhong Liu and Jiang-Da He

State Key Laboratory of Hydraulics and Mountain River Engineering, College of Water Resource and Hydropower, Sichuan University, Chengdu 610065, China

\* Correspondence: zhuoli@scu.edu.cn

**Abstract:** Landslides are usually caused by rainstorms and geological processes such as earthquakes and may have a massive impact on human production and life. The hazard chain of landslide–river blockage–outburst flood is the most common hazard chain caused by landslides. A database based on existing landslide cases was established in this study to investigate the assessment formulas of the risk of river blockage, dam stability, and peak flood discharge after a dam has broken. A risk assessment model of the landslide–river blockage–breaching hazard chain was established, including the downstream vulnerability. The case of the Baige landslide verified the applicability of the model. This model can be used in a landslide-prone area to predict whether a relatively massive river blockage will form after the landslide occurs, whether the landslide dam formed by the river blockage will breach in a short time, and the impact of the outburst flood on the downstream area.

**Keywords:** river blockage; landslide dam; breaching flood; hazard chain; risk assessment



**Citation:** Yang, F.-Y.; Zhuo, L.; Xiao, M.-L.; Xie, H.-Q.; Liu, H.-Z.; He, J.-D. A Statistical Risk Assessment Model of the Hazard Chain Induced by Landslides and Its Application to the Baige Landslide. *Appl. Sci.* **2023**, *13*, 3577. <https://doi.org/10.3390/app13063577>

Received: 6 February 2023

Revised: 8 March 2023

Accepted: 9 March 2023

Published: 10 March 2023



**Copyright:** © 2023 by the authors. Licensee MDPI, Basel, Switzerland. This article is an open access article distributed under the terms and conditions of the Creative Commons Attribution (CC BY) license (<https://creativecommons.org/licenses/by/4.0/>).

## 1. Introduction

The natural hazard chain refers to a series of secondary hazards induced by a single natural hazard [1]. Compared with a single hazard, a hazard chain has the characteristics of a long time scale, broad scope, and immense destructiveness and results in enormous losses of life and economic losses, and harmful social and environmental effects [2]. Heavy rains, debris flows, earthquakes, landslides, landslide dams, and outburst floods are all individual hazards, but sometimes, they can be in a hazard chain and cause more severe hazards. A landslide is usually caused by heavy rains or geological effects such as earthquakes and occurs suddenly, with huge impacts on human production and life [3]. When there is a river in the direction of the landslide, the landslide can easily block the river and form a landslide dam. The landslide dam causes the upstream water level to keep rising and also causes the submersion of the upstream residential area. Once the landslide dam breaches, the large amount of water accumulated in the barrier lake will be released quickly and will cause enormous hazards downstream.

In recent years, frequent earthquakes and heavy rains have led to a global outbreak of landslides [4]. The Tangjiashan landslide dam formed in the 2008 Wenchuan earthquake and collapsed 29 days later. The dam forced nearly 200,000 people downstream to evacuate [5]. In 2009, heavy rainfall caused by a typhoon led to landslides and debris flows in Hsiaolin Village. The landslides buried the village and blocked the gorge of the Cishan River, and the peak outflow rate reached 70,649 m<sup>3</sup>/s after the landslide dam breached [6]. In 2018, landslides blocked the Jinsha River twice at the same location. The outburst flood caused road damage and extensive damage to large areas of farmland and houses [7].

Therefore, a risk assessment method needs to be proposed to reduce the economic loss, loss of life, and social and environmental effects of the hazard chain. In the existing research, scholars from China and overseas have mostly used mathematical methods, such as the

analytic hierarchy process, the Poisson probability model, and information models, to evaluate the vulnerability and risk of landslide disasters. However, the existing risk assessments have focused primarily on single hazards, including forecasts of landslide movements [8,9], dam formation [10–13], dam stability [14–17], and outburst floods [3,10,18,19]. With the development of science and technology, more and more advanced methods are used for forecasting hazards. Ji et al. [20] proposed the inverse FORM algorithm and, based on this, a geographic information system extension tool was developed for probabilistic physical modeling and forecasting landslides [21]. Panagoulia [22,23] analyzed the responses of the medium-sized mountainous Mesochora catchment to climate change and proposed a multi-stage method for selecting input variables for ANN forecasts of river flows.

For assessing the risk of a hazard chain, a conceptual risk assessment model of a regional hazard chain was proposed based on Newmark's permanent deformation model and applied to predicting a disaster chain induced by the Wenchuan earthquake [24]. Dong [25] summarized the hazard chain mode of river blockages induced by avalanches on the basis of a hazard chain structure. A risk assessment of the Layue landslide dam was carried out from the aspects of risk and vulnerability. These studies have mainly focused on the concept of a hazard chain, but have yet to emphasize a systematic risk assessment model. Although the remedy for a hazard chain lies in blocking it before expansion/transformation, sometimes, it is inevitable [26]. Therefore, a risk assessment model is needed to reduce the losses caused by the hazard chain.

This study aimed to explore a risk assessment model of hazard chains and to apply it to the case of landslides. A database was established for statistical analysis. Based on existing research, formulas were established for assessing the risk of river blockages caused by landslides, the stability of landslide dams, and the peak flood discharge after dam breakage. A risk assessment model of the hazard chain of landslide–river blockage–outburst flood was proposed, with explicit formulas. The case of the Baige landslide was investigated to verify the applicability of the model.

## 2. Statistical Analyses of Individual Hazards

The evolution of the investigated hazard chain caused by landslides can be divided into three stages: river blockage, dam breakage, and the outburst flood. The risks of these three hazards are accessed individually in this section. A database including 57 landslide events, 50 historically documented landslide dams, and 34 landslide dam breaches was established with relatively complete and accurate data. Some improved risk assessment models were proposed and calibrated on the basis of the database.

### 2.1. Risk Assessment of River Blockage Caused by Landslides

The river blockage caused by landslides can be classified into complete blockage and partial blockage, as shown in Figure 1. In the case of a partial blockage, the landslide deposit blocks part of the river channel and the river still flows through the unblocked channel. In the case of a complete blockage, the landslide deposit completely blocks the river channel and forms a landslide dam, which promotes the formation of a barrier lake. Therefore, assessing the degree of river blockage is the primary task of risk assessment.

Tacconi Stefanelli et al. [13] investigated the relationship between the formation of landslide dams and two critical conditions, namely landslide volume and valley width, and proposed an assessment index, named the morphological obstruction index (MOI), as follows:

$$\text{MOI} = \lg(V_L/W_V) \quad (1)$$

where  $V_L$  denotes the landslide's volume ( $\text{m}^3$ ) and  $W_V$  denotes the valley's width (m). When  $\text{MOI} > 4.6$ , a landslide dam forms; when  $\text{MOI} < 3.00$ , a landslide dam does not form; and landslide dams are uncertain when  $3.00 \leq \text{MOI} \leq 4.6$ . The advantage of this formula is that the valley's width and the landslide's volume can easily be measured, so it is suitable for rapid assessments of the risk of river blockage.

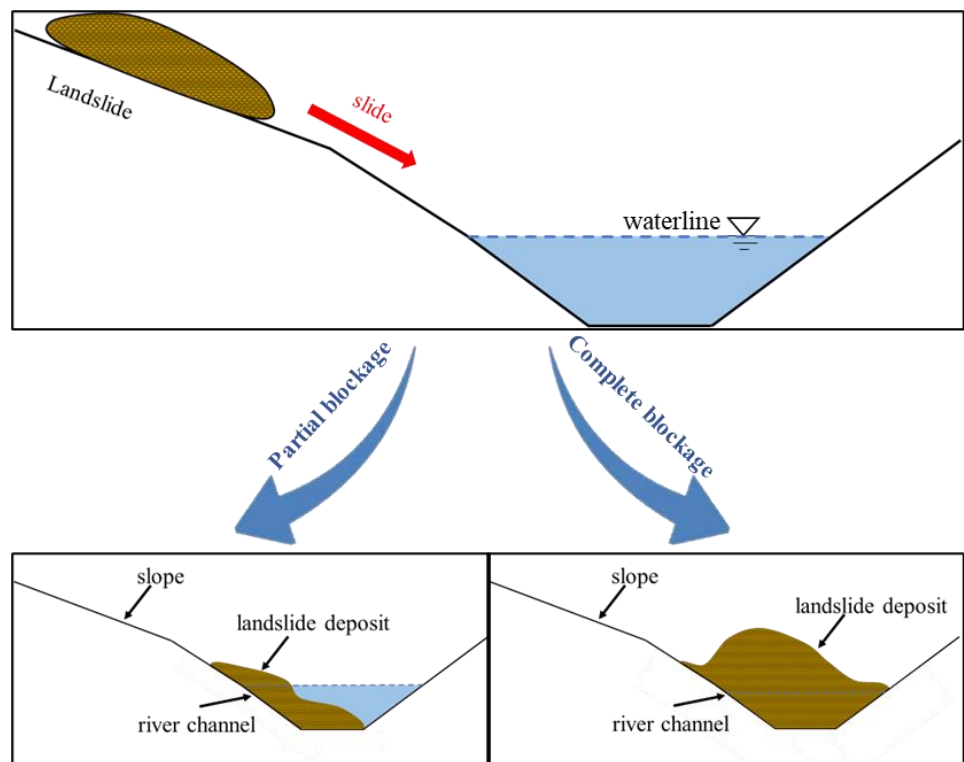


**Figure 1.** The difference between complete blockage and partial blockage.

However, the accuracy of the MOI is poor. Only 57.9% of the cases in the database could be assessed correctly (Table A1) by this method. This is because the risk of a landslide blocking the river is also related to many other factors, such as the valley’s shape, the riverbank’s slope, and the landslide’s materials. The accuracy needs to be improved by taking more factors into consideration.

A landslide formed on a steeper slope is more likely to induce a landslide dam, as the landslide generates more kinetic energy [10]. According to the database, the relationship between the steepness of the slope and the degree of river blockage can be statistically analyzed, as shown in Figure 2. This illustrates that a landslide with a steeper slope is more likely to completely block the river and form a landslide dam. Moreover, landslide materials with larger particles are also more likely to accumulate directly at the bottom of the river and form a landslide dam. It is also easier for a landslide dam to form in a V-shaped valley than in a U-shaped valley [27].

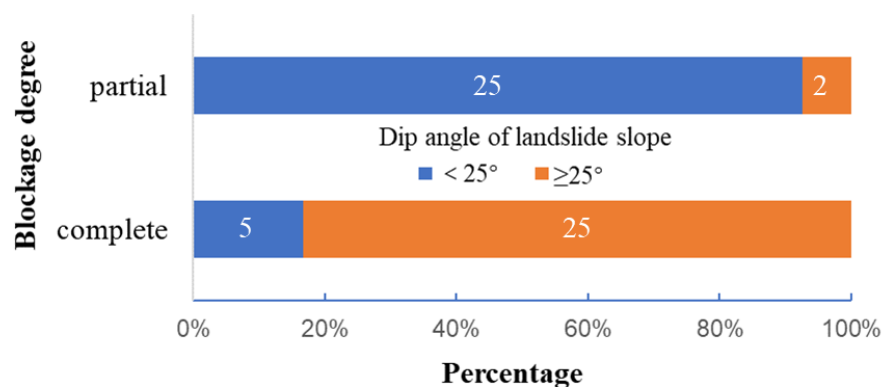


**Figure 2.** The percentages of landslide cases with different slope steepness, resulting in partial and complete river blockages.

Hu et al. [28] and Tacconi Stefanelli et al. [29] collected many cases of river blockages caused by landslides in China and Italy. Some cases with complete data were selected to establish a database of 57 events. According to the database (Table A1), an index based on the MOI was proposed, named the Landslide Blocking River Index (LBRI). The valley’s shape, the landslide’s materials, and the steepness of the slope were considered in the LBRI to make it more accurate and enhance its applicability. Because some cases lacked a description of the valley’s shape, the shapes of these cases were considered to be V-shape valleys for a conservative evaluation:

$$LBRI = \frac{A_C}{\cos \varphi} \log_{10}(V_L/W_V) \tag{2}$$

where  $\varphi$  denotes the steepness of the landslide slope ( $^\circ$ ) and  $A_C$  denotes the “accumulation coefficient”, which is related to the valley’s shape and the particle size of landslide materials. According to the analysis results of database, different values of  $A_C$  are suggested for various landslide materials and different valley shapes, as shown in Table 1.

**Table 1.** Suggested values of  $A_C$ .

Shape of Valley	Landslide Materials					
	Rock	Rock and Debris	Debris	Debris and Earth	Earth and Debris	Earth
V	1	0.95	0.9	0.85	0.8	0.75
U	0.9	0.85	0.8	0.75	0.7	0.65

In Figure 3, the results calculated for the LBRI were divided into two different domains, i.e., complete blockage and partial blockage. According to the statistical analysis of these data, when  $LBRI < 4.5$ , the river is partly blocked; when  $LBRI \geq 4.5$ , the river is completely blocked. When the number of correct cases was divided by the total number of cases, the formula’s accuracy reached 96.5%.

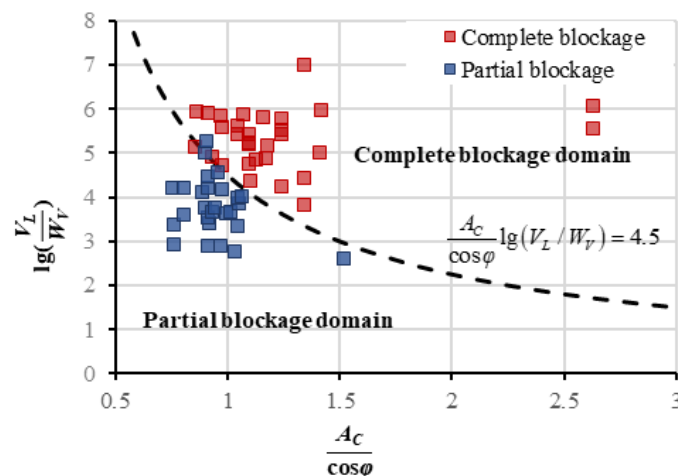


**Figure 3.** Critical conditions of river blockages caused by landslides.

### 2.2. Assessing the Stability of Landslide Dams

A landslide dam’s stability increases with the dam’s volume or the ratio of the dam’s width to its height. Obviously, the longer the dam is, with the higher hydraulic thrust, the lower the stability of the dam will be. Meanwhile, as the ratio of the reservoir capacity of the barrier lake to the dam’s volume increases, the landslide dam’s stability decreases [30]. Canuti et al. [14] proposed the blockage index (BI) to assess a dam’s stability. The formulation of BI is expressed as follows:

$$BI = \log_{10} \left( \frac{V_D}{S_C} \right) \tag{3}$$

where  $V_D$  is the dam’s volume ( $m^3$ ) and  $S_C$  is the catchment area ( $10^6 m^2$ ). Canuti et al. [14] suggested that when  $BI > 5$ , the dam is stable; when  $4 \leq BI \leq 5$ , the stability is unsure; and when  $3 < BI < 4$ , the dam is unstable.

The dam volume is easily measured, and the catchment area is easily calculated. The BI is instructive for the rapid assessment of the stability of landslide dams, so it is widely used [13,16,31]. However, the accuracy of the BI is poor. Only 50.0% of the cases in the database could be assessed correctly (Table A2).

Xu [17] developed a rapid assessment model of the stability of landslide dams by collecting the geometric information and breach times of 110 landslide dams worldwide. The model consists of two parts [17], i.e., Fisher’s discriminant model  $Y_A$  and the logistics regression model  $Z_B$ .

$$Y_A = -8.935 + 2.453 \log_{10} H_d - 0.832 \log_{10} V_D + 0.4911 \log_{10} V_l + 0.471 \log_{10} S_C \tag{4}$$

$$Z_B = -8.542 + 3.704 \log_{10} H_d - 0.732 \log_{10} V_D + 0.801 \log_{10} S_C \tag{5}$$

where  $V_l$  is the reservoir capacity of the barrier lake ( $m^3$ ) and  $H_d$  is the dam’s height (m).

Fisher’s discriminant model considered the influences of the dam’s height  $H_d$ , the landslide dam’s volume  $V_D$ , the reservoir capacity of the barrier lake  $V_l$ , and the catchment area  $S_C$  on the stability of landslide dams. The logistic regression model considered the influences of the dam’s height  $H_d$ , the landslide dam’s volume  $V_D$ , and the catchment area  $S_C$  on the stability of landslide dams. In Fisher’s discriminant model, if  $Y_A < 0$ , the landslide dam is stable; if  $Y_A > 0$ , the landslide dam is unstable. In the logistic regression model, if  $Z_B < 0.5$ , the landslide dam is stable; if  $Z_B > 0.5$ , the landslide dam is unstable.

Dam materials originate from the landslide’s materials, so they have almost the same material composition. Dams made up of earth or soft rock have a low shear strength and are prone to breaching, and dams made up of rock or debris are more stable [32]. Therefore, it is also necessary to consider the influence of the dam materials.

### 2.2.1. The Landslide Dam Stability Index

Shan et al. [16] established a database for rapid predictions of dam stability. In the database, 50 documented historical landslide dams with complete data were chosen for assessing the stability of landslide dams, as listed in Table A2. Based on Xu’s model and the database, a new index named the landslide dam stability index (LDSI) was proposed, which is expressed as follows:

$$LDSI = \frac{\log_{10} \frac{100H_d L_d V_l^{\frac{1}{3}} S_C^{\frac{1}{2}}}{W_d V_D}}{M} \tag{6}$$

where  $W_d$  is the dam’s width (m),  $L_d$  is the dam’s length (m), and  $M$  is the material coefficient, which describes the influence of the material on the dam’s stability. If the geometries of two landslide dams are exactly the same, a landslide dam formed by rock is more stable than one formed by earth, so the deposited material significantly affects the stability. Different values of  $M$  have been suggested for various landslide materials according to the results of analyzing the database. The suggested values of  $M$  are listed in Table 2.

**Table 2.** Suggested values of  $M$ .

Rock	Rock and Debris	Debris	Debris and Earth	Earth and Debris	Earth
1.0	0.9	0.8	0.7	0.6	0.5

Figure 4 shows that when  $LDSI < 2.7$ , the landslide dam is stable, and when  $LDSI \geq 2.7$ , the landslide dam is unstable. When the number of correct cases was divided by the total number of cases, the formula's accuracy reached 86%.

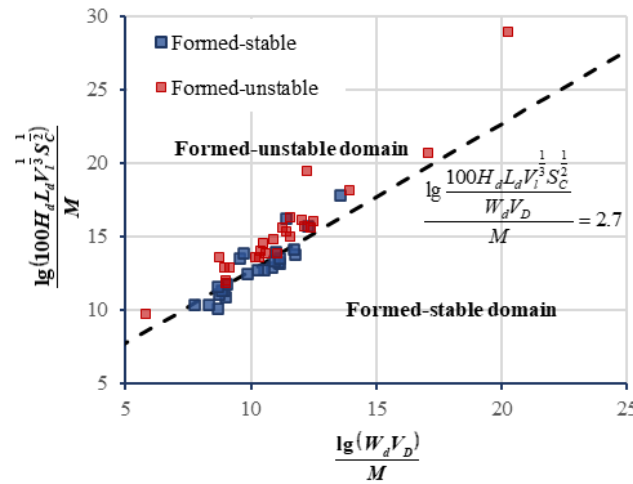


Figure 4. Critical conditions for the stability of landslide dams.

Before a landslide occurs, it is difficult to precisely evaluate the dam's length, height, width, and volume; the reservoir capacity of barrier lake; catchment area; etc. Thus, to assess the risk of the hazard chain triggered by a landslide, it is necessary to estimate these parameters in advance. Some empirical methods are introduced in the following section.

### 2.2.2. Some Methods of Calculating the Parameters

Equation (6) involves the dam's height, width, length, and volume; the reservoir capacity of the barrier lake; the catchment area; and the material coefficient. Only the material coefficient is known. Chen et al. [33] studied the landslide events in Taiwan and proposed a formula for the volume of a dam. However, the formulas were proposed on the basis of rainfall and earthquake conditions. On the basis of the form of this formula and the database, a new formula for calculating the volume of a dam in all cases is as follows:

$$V_D = 3.057V_L^{0.363} \tag{7}$$

where  $V_D$  has a unit of  $10^6$  m and  $V_L$  has a unit of  $10^6$  m. The fitting results show that Equation (7) has a correlation coefficient of 0.675.

According to the results when analyzing the database, the dam's width is mainly affected by the dam's volume and has little correlation with the dam's height. A formula for the dam's width can be fitted as follows:

$$W_d = 0.00592V_D^{0.746} \tag{8}$$

The fitting results of the database show that Equation (8) has a correlation coefficient of 0.850.

Hu et al. [28] proposed an empirical formula based on 86 cases to calculate the length of a dam:

$$L_d = 224.87 - 1.915 \times 10^{-3}V_L^2 - 0.056h^2 + 6.8V_L + 8.683h \tag{9}$$

where  $h$  is the depth of water in the river (m).

After the volume, width, and length of the dam have been determined, the height of the dam can be easily calculated as follows:

$$H_d = 0.426 \times \frac{V_D}{W_d^{0.84}L_d^{0.85}} \tag{10}$$

The fitting results of the database show that Equation (10) has a correlation coefficient of 0.799.

The geometric relationship for estimating the reservoir capacity of the barrier lake and the catchment area is shown in Figure 5. The reservoir capacity of the barrier lake and the catchment area can be calculated as follows:

$$V_l = \frac{H_d^2 L_d}{6 i_u}, \text{ for V – shaped valley} \quad (11)$$

$$V_l = \frac{H_d^2 L_d}{2 i_u}, \text{ for U – shaped valley} \quad (12)$$

$$S_C = \frac{H_d L_d}{2 i_u}, \text{ for V – shaped valley} \quad (13)$$

$$S_C = \frac{H_d L_d}{i_u}, \text{ for U – shaped valley} \quad (14)$$

where  $i_u$  is the upstream riverbed's inclination along the river (rad).

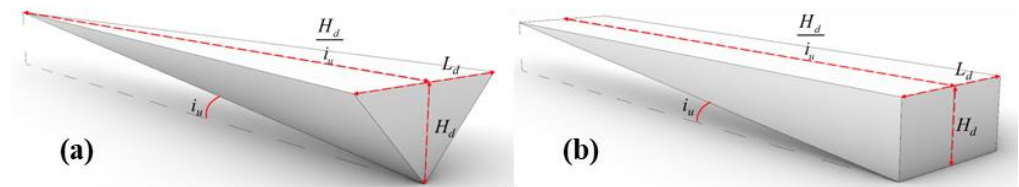


**Figure 5.** Schematic diagram for estimating the reservoir capacity of a barrier lake. (a) V-shaped valley. (b) U-shaped valley.

### 2.3. Assessment of the Peak Flood Discharge after a Dam Breake

After the dam has been breached, the peak outflow rate occurs at the dam site, and the peak flood discharge decreases with an increase in the distance of the flow. The degree of risk is assessed by comparing the relationship between the peak flood discharge, the check flood discharge, and the average annual discharge in a downstream area.

Based on 12 cases of landslide dams, Costa and Schuster [10] established the relationship between the peak outflow rate and potential energy:

$$Q_p = 0.0158(PE)^{0.60} \quad (15)$$

$$PE = V_l \times H_d \times \gamma_w \quad (16)$$

where  $PE$  is the potential energy (N·m) and  $\gamma_w$  is the specific gravity of water (N/m<sup>3</sup>).

#### 2.3.1. The Method of Calculating the Peak Outflow Rate

The higher the landslide dam or the larger the reservoir capacity of the dam lake, the more potential energy will be stored in the dam. Because the shape of the breach is difficult to predict, the development process of the breach can be ignored, and the relationship between the influences of some related factors on the peak outflow rate can be estimated on the basis of a statistical analysis of the cases of dam breaches.

The estimation model proposed by Costa and Schuster [10] should be improved by considering the influencing factors of the dam's volume and its erodibility. According to the 34 dam breaching cases listed in Table A3, a new formula is proposed:

$$\begin{cases} Q_p = \frac{\beta \times (V_l \times H_d \times \gamma_w)^{0.5}}{V_D}, & H_d \leq 20 \text{ m} \\ Q_p = \beta \times (V_l \times H_d \times \gamma_w)^{0.5}, & H_d > 20 \text{ m} \end{cases} \quad (17)$$

where  $\beta$  is the coefficient of the erodibility related to the dam materials. According to the results of analyzing the database, the suggested values of  $\beta$  are listed in Table 3.

**Table 3.** Suggested values of  $\beta$ .

Dam Material	Erodibility of the Dam	$\beta$
Rock Rock and debris	Low	$2.2 \times 10^{-4}$
Debris Earth and debris Debris and earth	Medium	$8 \times 10^{-4}$
Earth	High	$2 \times 10^{-3}$

Figure 6 shows a comparison between the measured peak outflow rate and the calculated peak outflow rate, and presents a good degree of fitting with a correlation coefficient of 0.934. However, the correlation coefficient of Costa and Schuster’s formula only reached 0.787 in this database.

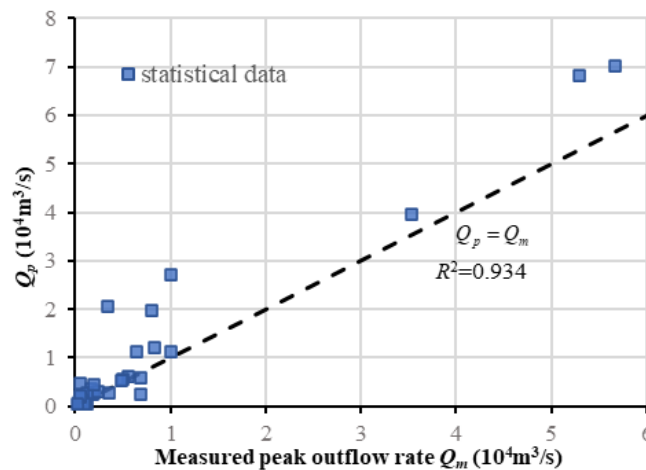


**Figure 6.** Comparison between the measured peak outflow rate and the calculated peak outflow rate.

### 2.3.2. The Method of Calculating the Downstream Peak Flood Discharge

Li [34] proposed an empirical formula called the attenuation formula of the peak outflow rate to predict the peak flood discharge somewhere downstream:

$$Q_{L_0} = \frac{V_l}{\frac{V_l}{Q_p} + \frac{L_0}{V_{\max}K}} \tag{18}$$

where  $L_0$  is the distance from the dam site to somewhere downstream (m),  $Q_{L_0}$  is the peak flood discharge at  $L_0$  from the dam site ( $m^3/s$ ), and  $V_{\max}$  is the maximum average flow velocity during the flood period (m/s). The historical maximum velocity can be used in the areas with detailed data. If there are no data, Li [34] suggests that 3.0–5.0 m/s can be used in general mountainous areas, 2.0–3.0 m/s in semi-mountainous areas, and 1.0–2.0 m/s in plains.  $K$  is an empirical coefficient. Li [34] also suggests that  $K$  equals 1.1–1.5 in mountainous areas, 1.0 in semi-mountainous areas, and 0.8–0.9 in plains.

If we compare  $Q_{L_0}$  to the check flood discharge  $Q_{max}$  and the average annual discharge  $\bar{Q}$ , the safety index ( $S_i$ ) can be obtained. The formulation of  $S_i$  is expressed as follows:

$$S_i = \begin{cases} 0 & Q_{L_0} \leq \bar{Q} \\ \frac{Q_{L_0} - \bar{Q}}{Q_{max} - \bar{Q}} & \bar{Q} < Q_{L_0} \leq Q_{max} \\ \frac{Q_{L_0}}{Q_{max}} & Q_{max} < Q_{L_0} \end{cases} \quad (19)$$

### 3. Risk Assessment Model

Based on the classical risk assessment model, the risk assessment model of the hazard chain triggered by a landslide was established as follows:

$$R = H \times V \quad (20)$$

where  $R$  is the index of the degree of risk,  $H$  is the hazard assessment index, and  $V$  is the vulnerability assessment index.

#### 3.1. Hazard Assessment Index

A hazard assessment assesses the possibility of a hazard by comprehensively considering the degree of river blockage, the stability of the landslide dam, and the peak outflow rate. The assessment coefficients are usually normalized in risk assessments. Therefore, the coefficients  $A$  for LBRI and  $B$  for LDSI are normalized as follows:

$$A = \begin{cases} \frac{LBRI}{4.5} & LBRI < 4.5 \\ 1 & LBRI \geq 4.5 \end{cases} \quad (21)$$

$$B = \begin{cases} \frac{LDSI}{2.7} & LDSI < 2.7 \\ 1 & LDSI \geq 2.7 \end{cases} \quad (22)$$

The hazard assessment formula can then be expressed as follows:

$$H = A \times B \times S_i \quad (23)$$

#### 3.2. Vulnerability Assessment

Vulnerability refers to the social and environmental impacts, loss of life, and economic losses caused by hazards. The relationship among the factors of vulnerability assessments and their classifications are listed in Table 4, and the values of the vulnerability factors are in Table 5 [35].

**Table 4.** The factors of vulnerability and their classifications.

Vulnerability Factors			Vulnerability Classification			
Type	Symbol	Factor	I	II	III	IV
Loss of life	<i>RP</i>	Risk population	$\leq 10^4$	$10^4 - 10^5$	$10^5 - 10^6$	$\geq 10^6$
Economic loss	<i>PG</i>	GDP per capita (CNY)	$\leq 10,000$	10,000–40,000	40,000–70,000	$\geq 70,000$
Social and environmental impacts	<i>UH</i>	Urban hierarchy	Village	Township	Town	County and above
	<i>FL</i>	Facility level	Common	Municipal	Provincial level	National level

Note: The economic loss was classified according to China’s GDP per capita in 2021. This indicator could also be revised on the basis of the economic development of different countries.

**Table 5.** The values of different vulnerability factors.

Factor	Vulnerability Classification			
	I	II	III	IV
RP	0–0.5	0.5–0.75	0.75–1.0	1.0
PG	0–0.5	0.5–0.75	0.75–1.0	1.0
UH	0.25	0.5	0.75	1.0
FL	0.25	0.5	0.75	1.0

According to the research of Liu et al. [35], the vulnerability assessment formula is expressed as follows:

$$V = 0.5RP + 0.1PG + 0.2UH + 0.2FL \tag{24}$$

The weight coefficients of the vulnerability assessment are determined according to the degree of influence of each factor. Losses of life are the most serious losses in all kinds of geological hazards and have the highest weight. The recovery of economic losses is faster than the recovery from social and environmental impacts, so it has the lowest weight. Therefore, the weight coefficients were adjusted on the basis of the research of Liu et al. [35].

### 3.3. Risk Assessment

Figure 7 shows the operational procedure of the model, which is divided into five steps. In the first step, LBRI is used to obtain the value of A. In the second step, LDSI is used to obtain the value of B. In the third step,  $S_i$  is used to assess the degree of the risk of a breaching flood. In the fourth step, V is used to assess the vulnerability of the downstream area. Finally, the value R is acquired for assessing the level of risk.

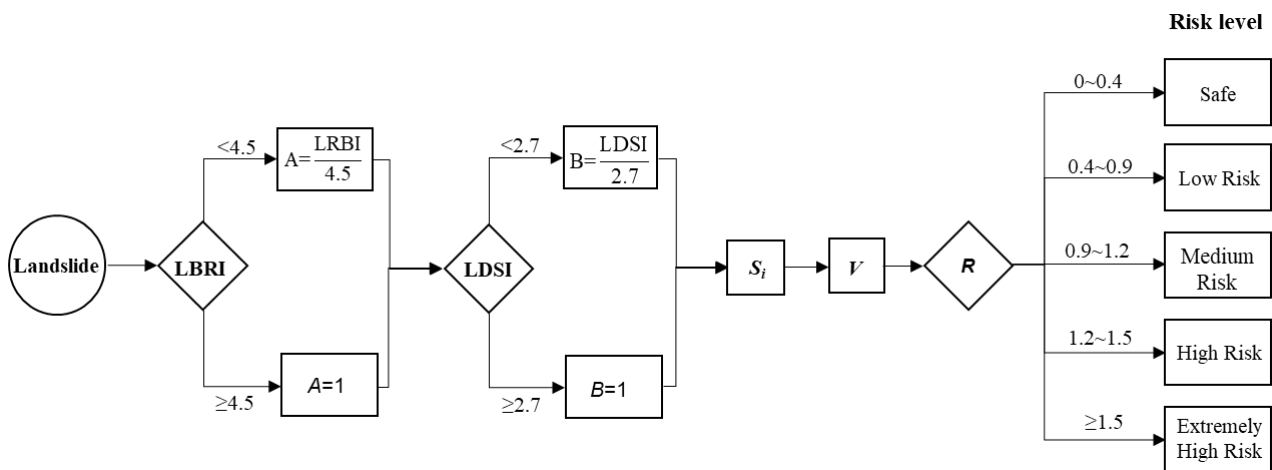


**Figure 7.** Flow chart of the risk assessment model.

## 4. Application

On 10 October 2018, a huge landslide composed of earth and debris occurred in Baige Village at the junction of Sichuan Province and Tibet in China. Figure 8 shows an overhead view of the Baige landslide and the landslide dam before it breached. The main channel of the Jinsha River was blocked, and a vast landslide dam was formed. The maximum reservoir capacity of barrier lake reached  $2.9 \times 10^8 \text{ m}^3$  [7], which seriously threatened the lives and properties safety of the residents downstream.

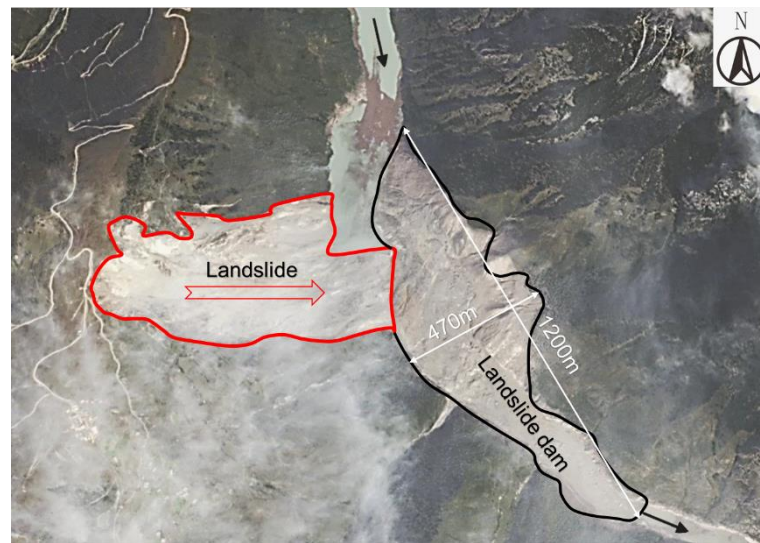


**Figure 8.** Overhead view of the Baige landslide and the landslide dam (photo credit: Yangtze River Water Resources Commission).

4.1. Landslide Parameters

According to the literature [7,36–42], the Baige landslide had some characteristic parameters, as listed in Table 6.

**Table 6.** Measured parameters of the river channel and the landslide dam.

Parameter	Value	Parameter	Value
Width of the valley $W_V$ (m)	150	Reservoir capacity of the barrier lake $V_l$ ( $10^8$ m <sup>3</sup> )	2.9
Width of the dam $W_d$ (m)	1200	Average steepness of the landslide slope $\varphi$ (°)	33
Depth of the river $h$ (m)	10	Upstream riverbed slope $i_u$	0.00135
Height of the dam $H_d$ (m)	61	Volume of the dam $V_D$ ( $10^6$ m <sup>3</sup> )	10
Length of the dam $L_d$ (m)	470	Shape of the valley	V
Materials	Earth and debris	Volume of the landslide ( $10^6$ m <sup>3</sup> )	27.95

4.2. Risk Assessment

The first step was to calculate LBRI to assess the degree of river blockage. According to Table 1,  $A_C = 0.8$ . Using Equation (2), LBRI was found to be 5.027, thus the river was blocked completely and a landslide dam formed.

The Baige landslide was formed by gravitational deformation of several slopes during erosion of the river [43]. Equations (7)–(11) and (13) were used to predict the geometries of the landslide dam. The calculated and actual geometries are compared in Table 7.

**Table 7.** Calculated and actual geometries of the Baige landslide dam.

	$H_d$ (m)	$W_d$ (m)	$L_d$ (m)	$V_D$ ( $10^6$ m <sup>3</sup> )	$V_l$ ( $10^8$ m <sup>3</sup> )	$S_C$ ( $10^6$ m <sup>2</sup> )
Actual values	61	1200	470	10	2.9	—
Calculated values	67.21	1004.63	494.66	10.24	2.76	12.31

The calculated values were in good agreement with the actual values. According to Table 2,  $M = 0.6$ . Using Equation (6), LDSI was found to be 4.78, so the landslide dam was unstable.

The Baige landslide dam breached on 13 October 2018 (Figure 9). Because the value of  $H_d$  was 67.21 m,  $Q_p$  was calculated to be 10,786.35 m<sup>3</sup>/s, which is close to the actual value of 10,000 m<sup>3</sup>/s.



**Figure 9.** The breaching of the Baige landslide dam (photo credit: Yangtze River Water Resources Commission).

Yebatan hydropower station and Lawa hydropower station recorded comparatively detailed information, except for the maximum average flow velocity during the flood period [38,43]. The information recorded by the two hydropower stations and the results calculated using Equations (19) and (21)–(23) are listed in Table 8.

**Table 8.** The parameters and calculated results of the two hydropower stations.

Hydropower Station	$L_0$ (m)	$\bar{Q}$ (m <sup>3</sup> /s)	$Q_{max}$ (m <sup>3</sup> /s)	$K$	$V_{max}$ (m/s)	Actual Peak Flood Discharge (m <sup>3</sup> /s)	$Q_{L_0}$ (m <sup>3</sup> /s)	$H$
Yebatan	65,000	824	7430	1.5	5.0	7800	8057.32	1.084
Lawa	119,000	849	11,900	1.5	5.0	6600	6657.89	0.559

Yebatan hydropower station is a national facility. Nearby, there are two counties: Gongjue County and Baiyu County. The total population of the two counties is 110,000, and the GDP per capita is CNY 26361. Lawa hydropower station is also a national facility. Nearby, there are two counties: Kangmang County and Batang County. The total population of the two counties is 130,000, and the GDP per capita is CNY 35,613. According to Tables 4 and 5 and Equations (20) and (24), the values of the vulnerability factors and the risk level for the two hydropower stations were calculated and are listed in Table 9.

**Table 9.** Vulnerability factors for the two hydropower stations and their risk levels.

	$RP$	$PG$	$UH$	$FL$	$V$	$H$	$R$	Risk Level
Yebatan	0.753	0.636	1.0	1.0	0.8401	1.084	0.911	Medium
Lawa	0.758	0.713	1.0	1.0	0.8503	0.559	0.475	Low

In fact, only a local bank slope collapse occurred at the Yebatan hydropower station during the flood period and fortunately did not cause casualties. For the Lawa hydropower station, there was almost no impact. The calculated results were in line with the actual situation.

### 5. Discussion

For the case of the Baige landslide, the proposed assessment model was compared with other models, such as Equations (1), (3), and (15), for calculating the risks of river blockage, the dam’s stability, and the peak outflow rate. The results of this comparison are shown in Table 10. The analyzed results show that the proposed model had a more reasonable dam stability and peak outflow rate than the other two models, so it could have a higher accuracy in assessments of the risk of a landslide hazard chain.

**Table 10.** Comparison of the results for river blockages, dam stability, and peak outflow rate.

Assessment Stage	River Blockage		Dam Stability		Peak Outflow Rate	
Assessment content	MOI	LBRI	BI	LDSI	$Q_p$ (Equation (15))	$Q_p$ (Equation (17))
Calculated values	5.27	5.027	5.91	4.78	5,680,656 m <sup>3</sup> /s	10,786.35 m <sup>3</sup> /s
Predicted results	Complete blockage	Complete blockage	Stable	Unstable	—	—
Actual results	Complete blockage		Unstable		10,000 m <sup>3</sup> /s	

The high accuracy was because more factors were considered in the assessment formula. In this study, many factors were added, but some factors were not included, such as the difference in height between the landslide and the riverbed and the distance between the landslide and the river. These factors are very important in assessments of the risk of a landslide hazard chain, but have seldom been recorded in the existing database. Although the proposed model could fit the database in Appendix A very well, its applicability still needs to be verified with more detailed documented cases. More factors will be collected and added to the formulas to increase the accuracy of the assessments of the risk of a landslide hazard chain.

### 6. Conclusions

The hazard chain caused by a landslide is usually more harmful than the landslide itself. In this study, the most common hazard chain, namely landslide–river blockage–outburst flood, was studied.

According to 57 cases of landslide events, the formula for assessing the degree of river blockage was improved, and the accuracy rate in the studied cases reached 96.5%. According to 50 documented historical landslide dams, the discriminant formula of landslide dam stability was put forward, and the accuracy rate in the cases reached 86%. According to 34 cases of dam breaches, a formula for flood peak flow at the dam site was put forward, and the correlation coefficient  $R^2$  reached 0.934. A risk assessment model was proposed that combined the peak outflow rate attenuation formula and the improved vulnerability assessment index. The applicability of the proposed model was verified by the Baige landslide, and the calculated results were in good agreement with the measured results.

In practical applications, the advantage of this model is that it can be used to improve the efficiency of the emergency evacuation once a landslide has happened, as well as for increasing the level of engineering security in advance. However, the model has some limitations. Because of the lack of the corresponding measured data, factors such as the water content of landslide material, the river’s velocity, rainfall, and geological action after the landslide’s occurrence cannot be taken into account. The model should be improved regarding these aspects in subsequent research.

**Author Contributions:** All of the authors contributed to the study as follows. F.-Y.Y.: methodology, conceptualization, software, investigation, validation, writing—original draft, writing—review and editing. L.Z.: conceptualization; methodology; resources; writing—review and editing. M.-L.X.: conceptualization; methodology; writing—review and editing; funding acquisition. H.-Q.X.: methodology; writing—review and editing. H.-Z.L.: funding acquisition; writing—review and editing. J.-D.H.: supervision; writing—review and editing. All authors have read and agreed to the published version of the manuscript.

**Funding:** This work was supported by the National Key R&D Program of China (no. 2017YFC1501100), and the National Natural Science Foundation of China (no. 52109135).

**Institutional Review Board Statement:** Not applicable.

**Informed Consent Statement:** Not applicable.

**Data Availability Statement:** Data is contained in Appendix A.

**Conflicts of Interest:** The authors declare no conflict of interest.

### Appendix A. The Database

Hu et al. [28] and Tacconi Stefanelli et al. [29] collected many river blockage cases caused by landslides in China and Italy. A total of 57 river blockage cases with complete data are included in Table A1. Meanwhile, the calculation results of MOI and LBRI are included in the table for comparison.

**Table A1.** Landslide events with collected data and the value of LBRI.

No.	Country	Locality	Degree of Blockage	Landslide Material	Landslide Volume (m <sup>3</sup> )	Steepness of the Slope (°)	Valley Width (m)	Valley Shape	A <sub>C</sub>	MOI	LBRI
1	Italy	Roccella Valdemone	partial blockage	earth	150,000	11.3	180	—	0.75	2.92	2.23
2	Italy	Maranina	partial blockage	earth	700,000	11	310	—	0.75	3.35	2.56
3	Italy	Tassinaro	partial blockage	debris	100,000	10.7	130	—	0.9	2.89	2.64
4	Italy	Chiesa delle Grazie	partial blockage	rock and earth	180,000	11.8	230	—	0.95	2.89	2.81
5	Italy	S.Patrignano	partial blockage	rock stone	90,000	15.5	155	—	1	2.76	2.87
6	Italy	Voltre	partial blockage	debris and earth	1,000,000	9.1	260	—	0.8	3.59	2.90
7	Italy	Bardea	partial blockage	debris	200,000	12	80	—	0.9	3.40	3.13
8	Italy	Terrarossa	partial blockage	earth	475,000	9.1	30	—	0.75	4.20	3.19
9	Italy	Laurenzana	partial blockage	debris	300,000	9.9	90	—	0.9	3.52	3.22
10	Italy	Rosola	partial blockage	debris	1,000,000	4.3	180	—	0.9	3.74	3.38
11	Italy	Contr. Schiavone	partial blockage	debris and earth	6,000,000	7.4	385	—	0.8	4.19	3.38
12	Italy	Le Mottacce	partial blockage	debris	686,875	16	150	—	0.9	3.66	3.43

Table A1. Cont.

No.	Country	Locality	Degree of Blockage	Landslide Material	Landslide Volume (m <sup>3</sup> )	Steepness of the Slope (°)	Valley Width (m)	Valley Shape	A <sub>C</sub>	MOI	LBRI
13	Italy	Mineo-SudOvest	partial blockage	rock	170,000	17.4	80	—	1	3.33	3.49
14	Italy	Frassineta	partial blockage	debris	453,600	18	80	—	0.9	3.75	3.55
15	Italy	Roccella Valdemone-Ovest	partial blockage	rock and earth	479,700	17.3	115	—	0.95	3.62	3.60
16	Italy	Contr. Rocca Fisauli	partial blockage	debris and earth	7,000,000	17	550	—	0.85	4.10	3.65
17	Italy	Contr. Saracena	partial blockage	rock	750,000	10.2	170	—	1	3.64	3.70
18	Italy	Bettola	partial blockage	debris	5,781,250	11	375	—	0.9	4.19	3.84
19	Italy	Piazza Armerina-Nord	partial blockage	rock and earth	15,700	51.3	40	—	0.95	2.59	3.94
20	Italy	M.Piano del Pozzo III	partial blockage	rock	1,300,000	18.9	190	—	1	3.84	4.05
21	Italy	Ciano	partial blockage	debris	18,545,625	10	660	—	0.9	4.45	4.07
22	China	Yunyang	partial blockage	debris and earth	15,000,000	40	1000	U	0.75	4.18	4.09
23	Italy	Contr. Canseria	partial blockage	rock	1,540,693	17.3	160	—	1	3.98	4.17
24	Italy	Contr. Cugno Giovanni	partial blockage	rock	1,324,033	19.9	130	—	1	4.01	4.26
25	Italy	Contr. Vettrana	partial blockage	rock and earth	6,210,920	7.9	180	—	0.95	4.54	4.35
26	Italy	Bombiana	complete blockage	debris and earth	12,420,000	9.3	90	—	0.85	5.14	4.43
27	Italy	Randazzo-Nord	partial blockage	debris	18,421,333	0.7	190	V	0.9	4.99	4.49
28	China	Qiangjiangping	complete blockage	debris	24,000,000	31	300	U	0.8	4.90	4.58
29	Italy	Cerredolo	complete blockage	rock and debris	13,000,000	13.6	250	—	0.95	4.72	4.61
30	Italy	Serrazanetti	partial blockage	debris	18,125,000	9	100	—	0.9	5.26	4.79
31	China	Diexi1	complete blockage	rock	4,000,000	25	180	V	1	4.35	4.80
32	China	Shifang2	complete blockage	rock and debris	600,000	45	90	V	0.95	3.82	5.14
33	Italy	Frassinoro	complete blockage	debris and earth	109,769,494	11	125	—	0.85	5.94	5.15
34	China	Shimian	complete blockage	debris	3,000,000	35	55	V	0.9	4.74	5.20
35	China	Wanyuan	complete blockage	rock and debris	1,000,000	40	60	V	0.95	4.22	5.24
36	Italy	Corniglio	complete blockage	debris	200,000,000	10	250	—	0.9	5.90	5.39

Table A1. Cont.

No.	Country	Locality	Degree of Blockage	Landslide Material	Landslide Volume (m <sup>3</sup> )	Steepness of the Slope (°)	Valley Width (m)	Valley Shape	A <sub>C</sub>	MOI	LBRI
37	Italy	Bocassuolo	complete blockage	rock and debris	44,156,250	14	120	—	0.95	5.57	5.45
38	China	Beichuan	complete blockage	debris	2,000,000	45	30	U	0.8	4.82	5.46
39	Italy	Gropo	complete blockage	rock and debris	19,200,000	25	75	—	0.95	5.41	5.67
40	China	Lingzhi	complete blockage	earth	35,000,000	39.5	50	V	0.75	5.85	5.68
41	China	Yongsheng <sup>2</sup>	complete blockage	debris	13,000,000	35	85	V	0.9	5.18	5.70
42	China	Diexi <sup>2</sup>	complete blockage	debris	30,000,000	35	180	V	0.9	5.22	5.74
43	China	Wuxi	complete blockage	debris	7,650,000	40	100	V	0.9	4.88	5.74
44	China	Pingwu	complete blockage	rock and debris	16,000,000	25	40	V	0.95	5.60	5.87
45	China	Luzhou	complete blockage	rock and debris	15,600,000	30	60	V	0.95	5.41	5.94
46	China	Wulong	complete blockage	rock and debris	5,300,000	45	200	V	0.95	4.42	5.94
47	China	Yongsheng <sup>1</sup>	complete blockage	rock	12,000,000	32	85	V	1	5.15	6.07
48	China	Dazhou	complete blockage	debris	65,000,000	33	90	V	0.9	5.86	6.29
49	China	Luding	complete blockage	debris	248,750,000	35	400	V	0.95	5.79	6.72
50	China	Pailong	complete blockage	debris and earth	12,000,000	47	45	V	0.85	5.43	6.76
51	China	Jinshajiang	complete blockage	debris	22,480,000	40	70	V	0.95	5.51	6.83
52	China	Mianyang	complete blockage	rock	2,500,000	45	25	V	1	5.00	7.07
53	China	Koushan	complete blockage	rock and debris	150,000,000	40	250	V	0.95	5.78	7.17
54	China	Hanzhong	complete blockage	rock and debris	72,000,000	48	80	V	0.95	5.95	8.45
55	China	Yigong	complete blockage	rock and debris	300,000,000	45	30	V	0.95	7.00	4.58
56	China	Ludian	complete blockage	debris	12,000,000	70	35	V	0.9	5.54	4.61
57	China	Yajiang	complete blockage	debris	68,000,000	70	60	V	0.9	6.05	4.79

Note: <sup>1</sup> the first landslide in Yongsheng, <sup>2</sup> the second landslide in Yongsheng.

Shan et al. [16] established a database for the rapid prediction of dam stability. A total of 50 landslide dams with complete data are included in Table A2. Meanwhile, the calculation of BI and LRBI are included in the table for comparison.

**Table A2.** Landslide dams with measured data and the value of LDSI.

No.	Country	Name	Dam Height (m)	Dam Length (m)	Dam Width (m)	Dam Volume (10 <sup>4</sup> m <sup>3</sup> )	Lake Volume (10 <sup>6</sup> m <sup>3</sup> )	Catchment (km <sup>2</sup> )	Material	Stability	Material Coefficient	BI	LDSI
1	Italy	Alleghe	16	550	1375	550	15	248	Debris and bedrock	stable	1	4.35	1.04
2	Italy	Anterselva	45	960	1000	700	2.7	19.5	Rock and debris	stable	1	5.56	0.78
3	Italy	Antrona	50	900	1800	2000	6.7	40.8	Debris and rock	stable	1	5.69	0.83
4	Italy	Bribo (Riganati Stream)	30	150	350	75	5.668485	5	Debris and earth	unstable	0.8	3.91	1.34
5	Italy	Borta	70	600	1150	2300	91	190	Debris and bedrock	unstable	1	5.08	1.07
6	Italy	Bracca	4	530	350	40	0.2	29.6	Debris	unstable	1	4.13	0.70
7	Italy	Braies	20	540	900	800	5.52483	29	Rock and debris	stable	1	5.44	0.78
8	Italy	Cava 5. Giuseppe Nord	30	100	375	56.25	0.1	2.8	Rock	stable	1	5.18	0.96
9	Italy	Cava 5. Giuseppe Sud	30	100	550	82.5	0.1	0.6	Rock	stable	1	5.30	0.86
10	Italy	Cerredolo	35	250	500	437.5	13.188	341	Rock and debris	unstable	1	6.14	1.15
11	Italy	Contr. Bellicci	75	175	370	242.8125	0.18	6.3	Rock	stable	1	4.11	0.89
12	Italy	Contr. Lenzevacche	55	150	350	144.375	1.28333	13.8	Rock	stable	1	5.59	1.07
13	Italy	Contr.Monte	60	375	960	1080	2.2	6	Debris and bedrock	stable	1	5.02	0.80
14	Italy	Contr.Oliva	40	150	575	172.5	0.21	5	Rock	stable	1	6.26	0.92
15	Italy	Contr.Torazza	17.5	250	100	21.875	0.375	207.5	Earth and debris	unstable	0.8	5.54	1.32
16	Italy	Contr.Utra	75	150	450	253.125	2.47275	12.1	Rock	stable	1	3.02	1.09
17	Italy	Cucco(Serra Torrent)	12	200	270	30	1.8349375	7	Debris and earth	unstable	0.8	5.32	1.22
18	Italy	Cumi (Lago Stream)	40	560	750	800	28.574	44	Debris and earth	unstable	0.8	4.63	1.17
19	Italy	Draga	10	550	350	100	0.00785	4	Earth	unstable	0.4	5.26	1.05
20	Italy	Forni di Sotto	80	1100	1000	2000	250	131.8	Debris and bedrock	unstable	1	5.40	1.03
21	Italy	Gropo	80	150	875	1050	5.3	147.3	Rock and debris	unstable	1	3.96	1.19
22	Italy	Idro-Cima d'Antegolo	25	450	510	250	33.5	615.2	Debris	stable	1	5.18	1.19
23	Italy	Kummerse	50	300	600	600	5.75	85	Rock and debris	unstable	1	4.85	1.03
24	Italy	Lago Costantino	100	220	530	600	7	41	Debris and earth	stable	0.8	3.72	1.38
25	Italy	Lago Morto	40	540	2000	2000	23.69	17.2	Rock and debris	stable	1	3.61	0.88
26	Italy	Lizzano	15	225	500	200	8.4	83	Rock	unstable	1	4.21	1.05
27	Italy	Marro	25	190	470	120	9.42	38	Debris	unstable	1	4.85	1.15
28	Italy	Molveno	30	1300	3200	4000	161	73.1	Rock	stable	1	5.17	0.88
29	Italy	Pve S.Stefano	25	400	450	450	3	106.9	Rock and debris	unstable	1	6.07	0.89

Table A2. Cont.

No.	Country	Name	Dam Height (m)	Dam Length (m)	Dam Width (m)	Dam Volume (10 <sup>4</sup> m <sup>3</sup> )	Lake Volume (10 <sup>6</sup> m <sup>3</sup> )	Catchment (km <sup>2</sup> )	Material	Stability	Material Coefficient	BI	LDSI
30	Italy	Piaggiagrande-Renaio	15	90	100	10	0.002	1.3	Rock and debris	stable	1	4.38	0.71
31	Italy	Ponte Pia	20	200	480	85	3.76	582.7	Rock and debris	stable	1	4.50	1.30
32	Italy	Prato Casarile	40	200	450	175	0.3	1.5	Debris	stable	1	5.74	0.79
33	Italy	Ronchi	20	160	190	30	0.471	24.5	Debris	stable	1	4.62	1.05
34	Italy	Rovina	15	400	900	200	1.2	17.2	Debris and bedrock	stable	1	4.89	0.86
35	Italy	S.Cristina (Lago Stream)	50	450	850	1000	22.431375	21	Debris	unstable	1	3.16	0.93
36	Italy	Scanno	33.1	500	2000	1700	26	95	Bedrock	stable	1	6.07	1.01
37	Italy	Scascoli	5	30	70	1	0.03925	91	Bedrock	unstable	1	4.09	1.37
38	Italy	Schiazzano	15	40	65	2	0.00883125	5.6	Debris and earth	unstable	0.8	5.07	1.42
39	Italy	Sernio	43	300	930	200	22	891	Debris	unstable	1	5.68	1.42
40	Italy	Signatico	30	450	620	837	8	151.5	Debris	unstable	0.8	3.90	1.16
41	Italy	Tenno	50	900	650	1000	5	19.3	Debris	stable	1	5.25	0.73
42	Italy	Tovel	45	1300	1700	4000	7.37	40.4	Rock	stable	1	2.04	0.68
43	Italy	Tramarecchia	20	200	450	150	0.58	40.8	Bedrock (debris)	stable	1	3.55	0.96
44	Italy	Val Vanoi	40	500	1000	1000	18.2	167	Debris	unstable	1	3.35	1.03
45	Italy	Valderchia	9	110	160	10	0.0059346	4.5	Debris	unstable	1	4.74	0.81
46	Japan	Azusa River (1)	4.5	300	600	90	0.53	110	Andesite	stable	1	5.71	0.88
47	Japan	Hime River (1)	60	250	500	190	16	360	Andesite tuff breccia	unstable	1	6.00	1.34
48	Japan	Sai River	82.5	1000	650	2100	350	2630	Mudstone	unstable	0.4	4.57	2.97
49	USA	East Fork Hood River	11	100	225	10	0.105	11	Volcanic debris	unstable	1	4.78	1.08
50	USA	Jackson Creek Lake	4.5	975	317.5	77	2.47	47	Volcanic debris	unstable	1	4.35	0.67

Peng and Zhang [18] established a database of dam breaching cases. A total of 34 dam breaching cases with complete data worldwide are included in Table A3. Meanwhile, the calculations of  $Q_p$  are included in the table after the real peak outflow rate for comparison.

Table A3. Dam breaching cases with measured data and the value of  $Q_p$ .

No.	Name	Location	Dam Erodibility	Dam Height (m)	Dam Volume (m <sup>3</sup> )	Lake Volume (10 <sup>6</sup> m <sup>3</sup> )	Peak Outflow Rate (m <sup>3</sup> /s)	$Q_p$ (m <sup>3</sup> /s)
1	Totsu River, Nakatotsugawa Village	Japan	High	7	0.073	0.65	6900	7086.99
2	Arida River, Hanazono Village	Japan	High	10	0.18	0.047	890	923.75
3	Totsu River, Daito Village	Japan	High	10	0.23	0.93	3500	3215.83
4	Totsu River, Daito Village	Japan	High	18	0.036	0.78	3400	25,244.12
5	Nishi River, Totsugawa Village	Japan	High	20	0.63	0.4	1100	1088.89
6	Tsaticchhu	Bhutan	High	110	5	1.5	6900	2340.71
7	Tegemach River	U.S.S.R	High	120	20	6.6	4960	4969.84
8	Mantaro River	Peru	High	133	3.5	301	35,400	32,667.46

Table A3. Cont.

No.	Name	Location	Dam Erodibility	Dam Height (m)	Dam Volume (m <sup>3</sup> )	Lake Volume (10 <sup>6</sup> m <sup>3</sup> )	Peak Outflow Rate (m <sup>3</sup> /s)	Q <sub>p</sub> (m <sup>3</sup> /s)
9	Tanggudong	China	High	175	68	680	53,000	55,108.32
10	Bairaman River	Papua New Guinea	High	200	200	50	8000	16,786.29
11	Bireh-Ganga River	India	High	274	286	460	56,650	56,649.83
12	Arida River, Hanazono Village	Japan	Low	60	2.6	17	750	310.70
13	Ojika River	Japan	Low	70	3.8	64	620	604.71
14	Sho River	Japan	Low	100	19	150	1900	1831.20
15	Shiratani River, Totsugawa Village	Japan	Low	190	10	38	580	1289.17
16	Kano River, Kitatotsugawa Village	Japan	Medium	15	0.094	1.3	1600	4650.53
17	Kano River, Totsugawa Village	Japan	Medium	20	0.1	0.6	1300	3429.29
18	Nishi River, Totsugawa Village	Japan	Medium	20	0.6	1.3	980	841.30
19	Nishi River, Totsugawa Village	Japan	Medium	25	0.63	1.8	1200	346.73
20	Ram Creek	New Zealand	Medium	40	2.8	1.1	1000	343.25
21	Kaminirau River	Japan	Medium	50	2	2.2	440	518.42
22	Susobana River	Japan	Medium	54	1.2	16	510	1310.64
23	Pilsque River	Ecuador	Medium	58	1	2.5	700	587.04
24	Hime River	Japan	Medium	60	1.9	16	1800	1374.28
25	Tunawaea Landslide Dam	New Zealand	Medium	70	4	0.9	250	403.42
26	Naka River, Kaminaka Town	Japan	Medium	80	3.3	75	5600	3134.87
27	Totsu River, Amakawa Village	Japan	Medium	80	2.5	17	2400	1607.48
28	Totsu River, Daito Village	Japan	Medium	80	13	40	2000	2362.49
29	Tangjiashan	China	Medium	82	20.37	246.6	6500	5415.83
30	La Josefina	Ecuador	Medium	100	20	200	10,000	9556.15
31	Totsu River, Kitatotsugawa Village	Japan	Medium	110	3.1	42	4800	4729.52
32	Rio Paute	Ecuador	Medium	112	25	210	8250	10,329.48
33	Iketsu River	Japan	Medium	140	3.4	26	480	4218.10
34	Mantaro River	Peru	Medium	175	1300	670	10,000	22,333.80

## References

- Cui, Y.; Hu, J.; Xu, C.; Zheng, J.; Wei, J. A catastrophic natural disaster chain of typhoon-rainstorm-landslide-barrier lake-flooding in Zhejiang Province, China. *J. Mt. Sci.* **2021**, *18*, 2108–2119. [[CrossRef](#)]
- Xu, L.; Meng, X.; Xu, X. Natural hazard chain research in China: A review. *Nat. Hazards* **2013**, *70*, 1631–1659. [[CrossRef](#)]
- Shi, Z.; Ma, X.; Peng, M.; Zhang, L. Statistical analysis and efficient dam burst modeling of landslide dams based on a large-scale database. *Chin. J. Rock Mech. Eng.* **2014**, *33*, 1780–1790. [[CrossRef](#)]
- Chen, C.; Chang, J. Landslide dam formation susceptibility analysis based on geomorphic features. *Landslides* **2015**, *13*, 1019–1033. [[CrossRef](#)]
- Shi, Z.; Guan, S.; Peng, M.; Zhang, L.; Zhu, Y.; Cai, Q. Cascading breaching of the Tangjiashan landslide dam and two smaller downstream landslide dams. *Eng. Geol.* **2015**, *193*, 445–458. [[CrossRef](#)]
- Li, M.; Sung, R.; Dong, J.; Lee, C.; Chen, C. The formation and breaching of a short-lived landslide dam at Hsiaolin Village, Taiwan—Part II: Simulation of debris flow with landslide dam breach. *Eng. Geol.* **2011**, *123*, 60–71. [[CrossRef](#)]
- Zhang, X.; Xue, R.; Wang, M.; Yu, Z.; Li, B.; Wang, M. Field investigation and analysis on flood disasters due to Baige landslide dam break in Jinsha river. *Adv. Eng. Sci.* **2020**, *52*, 89–100. [[CrossRef](#)]

8. Gao, H.; Zhang, X. Landslide Susceptibility Assessment Considering Landslide Volume: A Case Study of Yangou Watershed on the Loess Plateau (China). *Appl. Sci.* **2022**, *12*, 4381. [\[CrossRef\]](#)
9. Shentu, N.; Yang, J.; Li, Q.; Qiu, G.; Wang, F. Research on the Landslide Prediction Based on the Dual Mutual-Inductance Deep Displacement 3D Measuring Sensor. *Appl. Sci.* **2023**, *13*, 213. [\[CrossRef\]](#)
10. Costa, J.; Schuster, R. The formation and failure of natural dams. *Geol. Soc. Am. Bull.* **1988**, *100*, 1054–1068. [\[CrossRef\]](#)
11. Dal Sasso, S.F.; Sole, A.; Pascale, S.; Sdao, F.; Bateman Pinzòn, A.; Medina, V. Assessment methodology for the prediction of landslide dam hazard. *Nat. Hazards Earth Syst. Sci.* **2014**, *14*, 557–567. [\[CrossRef\]](#)
12. Swanson, F.J.; Oyagi, N.; Tominaga, M. Landslide dams in Japan. *Landslide Dams: Process, Risk, and Mitigation*. ASCE **1986**, *3*, 131–145.
13. Tacconi Stefanelli, C.; Segoni, S.; Casagli, N.; Catani, F. Geomorphic indexing of landslide dams evolution. *Eng. Geol.* **2016**, *208*, 1–10. [\[CrossRef\]](#)
14. Canuti, P.; Casagli, N.; Ermini, L. Inventory of landslide dams in the Northern Apennine as a model for induced flood hazard forecasting. In *Proceedings of the Managing Hydro-Geological Disasters in a Vulnerable Environment*; CNR-GNDICI and UNESCO IHP: Perugia, Italy, 1998; pp. 189–202.
15. Ermini, L.; Casagli, N. Prediction of the behaviour of landslide dams using a geomorphological dimensionless index. *Earth Surf. Process. Landf.* **2003**, *28*, 31–47. [\[CrossRef\]](#)
16. Shan, Y.; Chen, S.; Zhong, Q. Rapid prediction of landslide dam stability using the logistic regression method. *Landslides* **2020**, *17*, 2931–2956. [\[CrossRef\]](#)
17. Xu, F. A rapid evaluation model of the stability of landslide dam. *J. Nat. Disasters* **2020**, *29*, 54–63. [\[CrossRef\]](#)
18. Peng, M.; Zhang, L. Breaching parameters of landslide dams. *Landslides* **2011**, *9*, 13–31. [\[CrossRef\]](#)
19. Walder, J.S.; O'Connor, J.E. Methods for predicting peak discharge of floods caused by failure of natural and constructed earthen dams. *Water Resour. Res.* **1997**, *33*, 2337–2348. [\[CrossRef\]](#)
20. Ji, J.; Zhang, C.; Gao, Y.; Kodikara, J. Reliability-based design for geotechnical engineering: An inverse FORM approach for practice. *Comput. Geotech.* **2019**, *111*, 22–29. [\[CrossRef\]](#)
21. Ji, J.; Cui, H.Z.; Zhang, T.; Song, J.; Gao, Y.F. A GIS-based tool for probabilistic physical modelling and prediction of landslides: GIS-FORM landslide susceptibility analysis in seismic areas. *Landslides* **2022**, *19*, 2213–2231. [\[CrossRef\]](#)
22. Panagoulia, D. Catchment hydrological responses to climate changes calculated from incomplete climatological data. In *Proceedings of the International Symposium on Exchange Processes at the Land Surface for a Range of Space and Time Scales*, Yokohama, Japan, 13–16 July 1993; pp. 461–468.
23. Panagoulia, D.; Tsekouras, G.J.; Kousiouris, G. A multi-stage methodology for selecting input variables in ANN forecasting of river flows. *Glob. Nest J.* **2017**, *19*, 49–57.
24. Zhou, H.; Wang, X.; Yuan, Y. Risk assessment of disaster chain: Experience from Wenchuan earthquake-induced landslides in China. *J. Mt. Sci.* **2015**, *12*, 1169–1180. [\[CrossRef\]](#)
25. Dong, X. Research on the Disaster Chain Modes of Avalanche and Landslide and the River Blocking Dam Risk Assessment. Master's Thesis, Chengdu University of Technology, Chengdu, China, 2016.
26. Zhao, H. The transforming mechanism of disaster chain/earth sciences edit committee. In *10000 Scientific Problems (Volume of Earth Sciences)*; Science Press: Beijing, China, 2010.
27. Ruan, H.; Chen, H.; Chen, J.; Cao, C.; Li, H. Review of investigation on hazard chain triggered by landslide blocking river and dam outburst flood. *Yellow River* **2022**, *44*, 56–64.
28. Hu, Y.; Xiao, M.; Xie, H.; Luo, Y. Statistical analysis and efficient dam key geometric parameters modeling of landslide dams based on database. *J. Nat. Disasters* **2021**, *30*, 122–132. [\[CrossRef\]](#)
29. Tacconi Stefanelli, C.; Catani, F.; Casagli, N. Geomorphological investigations on landslide dams. *Geoenvironmental Disasters* **2015**, *2*, 21. [\[CrossRef\]](#)
30. Zheng, H.; Shi, Z.; Shen, D.; Peng, M.; Hanley, K.J.; Ma, C.; Zhang, L. Recent Advances in Stability and Failure Mechanisms of Landslide Dams. *Front. Earth Sci.* **2021**, *9*, 659935. [\[CrossRef\]](#)
31. Shi, Z.; Shen, D.; Peng, M.; Zhong, Q.; Jiang, M. Research progress on rapid hazard assessment of landslide dams caused by landslides and avalanches. *Adv. Eng. Sci.* **2021**, *53*, 1–20.
32. Chai, H.; Liu, H.; Zhang, Z.; Liu, H. Preliminarily stability analysis of natural rock-field dam resulting from damming landslide. *Geol. Sci. Technol. Inf.* **2001**, *20*, 77–81.
33. Chen, K.; Kuo, Y.; Shieh, C. Rapid geometry analysis for earthquake-induced and rainfall-induced landslide dams in Taiwan. *J. Mt. Sci.* **2014**, *11*, 360–370. [\[CrossRef\]](#)
34. Li, W. *Hydraulic Calculation Manual*, 2nd ed.; China Water&Power Press: Beijing, China, 2006.
35. Liu, N.; Cheng, Z.; Cui, P.; Chen, N. *Dammed Lake and Risk Management*; Science Press: Beijing, China, 2013; p. 398.
36. Cai, Y.; Luan, Y.; Yang, Q.; Xu, F.; Zhang, S.; Shi, Y.; Yi, D. Study on structural morphology and dam-break characteristics of Baige barrier dam on Jinsha River. *Yangtze River* **2019**, *50*, 15–22. [\[CrossRef\]](#)
37. Deng, J.; Gao, Y.; Yu, Z.; Xie, H. Analysis on the formation mechanism and process of Baige landslides damming the upper reach of Jinsha River, China. *Adv. Eng. Sci.* **2019**, *51*, 9–16. [\[CrossRef\]](#)
38. Li, H.; Qi, S.; Chen, H.; Liao, H.; Cui, Y.; Zhou, J. Mass movement and formation process analysis of the two sequential landslide dam events in Jinsha River, Southwest China. *Landslides* **2019**, *16*, 2247–2258. [\[CrossRef\]](#)

39. Wu, B. Development principle of landslide and stability risk analysis of slop of reservoir bank of Buoluo hydroelectric power station in Jinsha River. Master Thesis, Chengdu University of Technology, Chengdu, China, 2008.
40. Wu, H.; Shan, Z.-G.; Nian, T.-K.; Ni, W.-D. Hazard Prediction Method of Landslide Damming and Analysis of a Typical Application. *IOP Conf. Ser. Earth Environ. Sci.* **2021**, *861*, 052014. [[CrossRef](#)]
41. Xie, C.; Chen, Q.; Hou, Q.; Hu, Y.; Zhou, J.; Fan, G. Numerical simulation of natural erosion and breaching process of “10·11” Baige landslide dam on Jinsha River. *Yangtze River* **2021**, *52*, 22–29.
42. Zhong, Q.; Chen, S.; Shan, Y. Numerical modeling of breaching process of Baige dammed lake on Jinsha River. *Adv. Eng. Sci.* **2020**, *52*, 29–37. [[CrossRef](#)]
43. Deng, J.; Chen, F.; Zhao, S.; Zhang, X. *Disaster Investigation of Baige Landslide*; Science Press: Beijing, China, 2021; p. 189.

**Disclaimer/Publisher’s Note:** The statements, opinions and data contained in all publications are solely those of the individual author(s) and contributor(s) and not of MDPI and/or the editor(s). MDPI and/or the editor(s) disclaim responsibility for any injury to people or property resulting from any ideas, methods, instructions or products referred to in the content.